Bulletin of the Seismological Society of America, Vol. 107, No. 3, pp. –, June 2017, doi: 10.1785/0120160271

*Short Note*

# A Cross-Correlation-Based Approach to Direct Seismogram Stacking for Receiver-Side Structural Inversion

by C. Sippl,* A. Kumar,† and J. Dettmer

**Abstract** Direct stacks of teleseismic waveforms recorded at a station have been used as an alternative to receiver functions for the retrieval of crustal 1D *S*-wave velocity models through inversion. Although they generally feature lower signal-to-noise ratios, their use has recently gained some attention because they do not rely on deconvolution. Avoiding deconvolution in waveform processing is a significant advantage for probabilistic (Bayesian) inversion methods that rely on a realistic assumption about the statistical distribution of waveform noise. However, the preservation of the effective source time function (STF) in the waveform data poses new challenges in the data processing. In this short note, we show that the simple technique that has been applied to directly stack waveforms to date lacks precision, because waveforms with emergent onsets or more complicated STFs are often stacked out of phase, which leads to artifacts in the stacked trace. We introduce a new cross-correlation-based stacking technique that avoids phase errors by stacking groups of mutually coherent traces and creating stacks for each of these families of traces. This separates the dataset into groups of events with similar STFs, which can be inverted jointly or separately.

*Electronic Supplement:* Figure of stacks for four additional global stations.

## Introduction

Receiver functions, that is, waveforms of teleseismic waves converted at receiver-side subsurface velocity discontinuities, have been used extensively for structural imaging and inversion for several decades (e.g., Vinnik, 1977; Langston, 1979). A recent development in receiver function inversion is the explicit calculation of uncertainties by also inverting for the noise level of the input trace in a hierarchical transdimensional Bayesian approach (Bodin *et al.*, 2012). This approach necessitates an assumption about the nature of the noise, that is, whether it follows a Gaussian, exponential, or other distribution. Whereas Gaussian noise can be considered a reasonable assumption for raw seismic traces, the deconvolution step in standard receiver function processing (e.g., Ammon, 1991; Ligorría and Ammon, 1999) changes the noise distribution in a way that is not generally understood, which leads to a tendency of underestimating uncertainties when applying the method of Bodin *et al.* (2012). Further research into transdimensional Bayesian inversion for receiver-side structure has thus focussed on direct seismogram inversion instead of receiver functions (Bodin *et al.*, 2014; Dettmer *et al.*, 2015). Leaving out the deconvolution step has the advantage of preserving the noise distribution but introduces additional complexity because the effective source time function (STF; i.e., moment release function plus radiation pattern and path effects) is retained in the traces that are inverted.

This short note focuses on the signal processing that is performed before an inversion algorithm is applied to the stacked seismogram data. Like receiver functions, direct seismograms are commonly stacked to enhance signal-to-noise ratio. Kumar *et al.* (2010), who first used directly stacked seismograms to visualize receiver-side converted phases, adapted a simple stacking procedure that Shearer (1991) had applied to global long-period data. Traces are aligned based on maximum phase amplitudes (*P* or *S*), normalized and summed up. In cases where the maximum amplitude is negative, the sign of the trace is reversed. However, we will show in this article that such a simple approach, possibly combined with back-azimuthal and/or slowness binning, as routinely used for receiver functions, can lead to artifacts in the stacked

*Now at Section Lithosphere Dynamics, German Research Centre for Geosciences (GFZ), Potsdam, Germany.
†Now at Institute of Earth Sciences Jaume Almera, CSIC, C/Lluis Sole Sabaris s/n, Barcelona, E-08028, Spain.

trace when applied to raw seismograms. Different raw traces that contain similar information about the receiver-side subsurface are convolved with different effective STFs (see Fig. 1), which has the effect that more complex traces are frequently stacked out of phase in the approach of Kumar *et al.* (2010). Because these out-of-phase traces are normally the exception rather than the rule, stacks still feature the converted phases at the correct time, but waveforms are modified, which adversely affects inversion. Dettmer *et al.* (2015) tried to address this problem by only looking at a very narrow range of magnitudes, assuming that effective STFs for these events would be similar, and then inverting for an average STF. However, earthquakes of similar magnitudes can still feature highly dissimilar effective STFs (see Fig. 1), with, for example, deep earthquakes showing systematically shorter STFs for the same magnitude (Houston, 2001). Here, we implement an alternative stacking approach that addresses these problems by not stacking all available waveforms from a station, but rather uses the similarity of waveforms as a criterion to define families of coherent traces that are then stacked separately. Each event family then consists only of traces with highly similar STFs. This stacking method avoids any "smearing out" of phases due to out-of-phase traces and thus produces sharper stacked waveforms, which allows a better identification of later phases (e.g., multiples).

## Method

We illustrate our method using recordings from the permanent station Hyderabad (HYB) in India, for which 18 years of continuous broadband data are available through the Incorporated Research Institutions for Seismology database. We choose HYB for ease of comparison with several previous publications that also considered HYB for waveform stacking (Kumar *et al.*, 2010; Bodin *et al.*, 2014; Dettmer *et al.*, 2015). Data include 3461 events with $\mathbf{M} > 5.5$ in the years 1990–2007. Traces were initially time windowed from 60 s before to 320 s after the theoretical *P* arrival, calculated using the global velocity model ak135 (Kennett *et al.*, 1995), then demeaned, detrended, downsampled to 10 Hz, and rotated into the ZRT (for *S* phase LQT) coordinate system. Finally, traces were band-pass filtered between 0.01 and 2 Hz and time windowed more narrowly around the theoretical *P* or *S* arrival (−30 to +150 s). The instrument response was not removed because it is identical for all traces utilized here. We then cross correlated (CC) a time window of 25 s length of the vertical-component (Q for *S* arrivals) velocity traces, from 10 s before to 15 s after the theoretical phase onset, allowing for a maximum time shift of 4 s between the traces. This maximum time shift was introduced to avoid cycle skipping and/or phase misidentification. CC coefficients and time shifts were stored for each combination of traces. In a last step, the matrix of CC coefficients is searched for populations of values higher than a threshold value (here 0.85 for *P* and 0.87 for *S*). The comparatively higher threshold value for *S* waveforms is due to

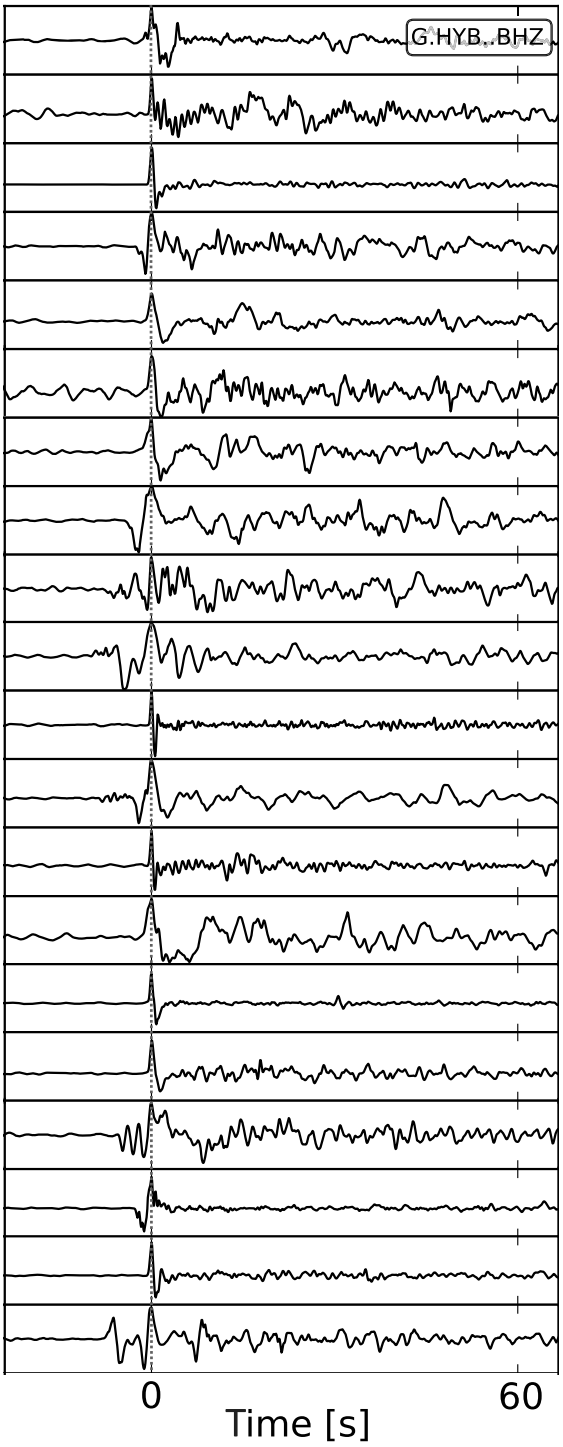


**Figure 1.** Vertical-component waveforms for *P* arrivals of 20 randomly selected teleseismic earthquakes, recorded at station HYB (Hyderabad) in India. Narrow ranges for back azimuth (50°–100°), epicentral distance (55°–75°), and magnitude (5.8–6.2) were used to choose equivalent earthquakes. These choices should reproduce the selection of traces performed in Dettmer *et al.* (2015). Traces are aligned with their maximum amplitude at 0 s; in cases of the maximum absolute amplitude being negative they were sign-reversed. It is evident that the waveforms show significant variety, and not all traces have their maximum amplitude in the first wiggle. Summing the traces up aligned like this will result in stacking artifacts.

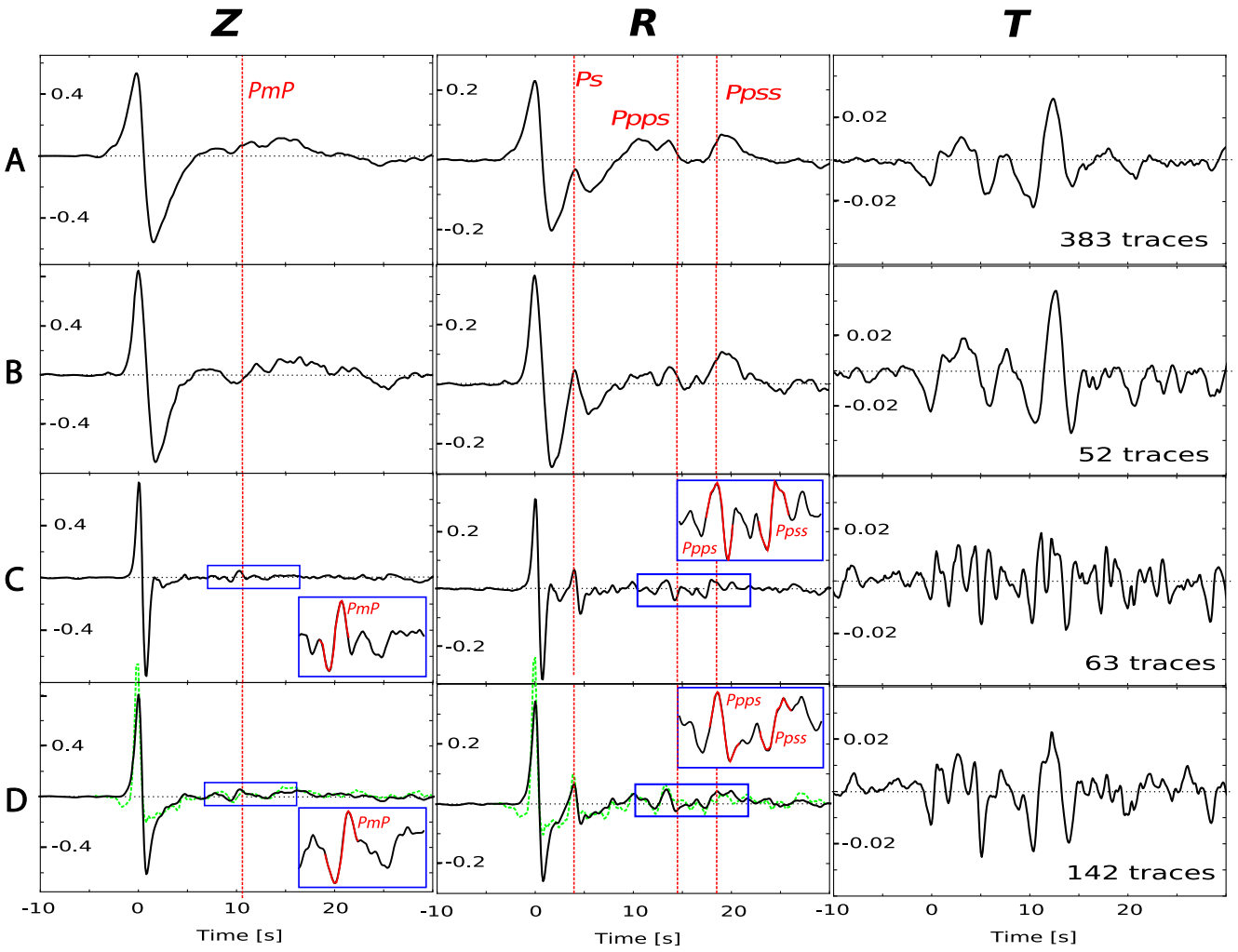


**Figure 2.** Stacked *P* arrivals for station HYB; the four stacks (families, labeled A–D) with most constituent traces are shown here, each row of the graph corresponding to one event family. Theoretical arrival times of conversion and reverberation phases, computed using Moho depth and average crustal velocities from Rai *et al.* (2003) ($d = 35$ km, $V_P = 6.62$ km/s, $V_S = 3.79$ km/s), are shown with vertical lines. The presented stacks were obtained by allowing all back azimuths and suitable epicentral distances (35°–95°); the only selection criterion was signal-to-noise ratio. Besides a very clear *Ps* phase that arrives at the predicted time, multiples (*Ppps* and *Ppss*) and *PmP* are also discernible for the event families with sharper source time functions (STFs; C+D, see magnified windows), all of them arriving somewhat earlier than theoretically predicted. Note that all phases show up as a narrow delta-like pulse convolved with the STF (up-then-down), with the phases that experienced an odd number of reflections off a faster medium *PmP*, *Ppss*) sign-reversed. The number of traces in each stack is displayed in the plot of the transverse (T) waveform. The vertical and radial stacks used for inversion in Dettmer *et al.* (2015) are plotted as a lighter line atop event family D for comparison; it can be seen that both the vertical and radial traces feature a negative precursory phase before the main *P* pulse that we do not retrieve with our method. The color version of this figure is available only in the electronic edition.

predominantly lower frequencies contained in the *S* wavetrain combined with the same length of the CC window. Typically, several families of mutually coherent traces are obtained, and we limit our analysis to stacks of at least 25 individual traces. The first trace in each family is defined as the reference trace, which is required to have a positive first pulse amplitude. All other traces of the family are then added to the reference trace after applying the CC-derived time shift; in the case of a negative CC coefficient relative to the reference trace, the traces are sign-reversed before addition. This is done for all three components (Z, R, and T or L, Q, and T), and all stacks are normalized by the amplitude of the stack of the reference phase (Z).

## Results

Figures 2 and 3 show a selection of stacks of *P* and *S* waveforms for station HYB. Unlike for the waveform examples in Figure 1, we did not constrain the back azimuth or magnitude of utilized events here, and allowed the use of all suitable epicentral distances (*P*: 35°–95°; *S*: 55°–75°). It is evident that the resulting stacks feature highly different pulse widths, which is due to different lengths of effective STFs. Although large events ($\mathbf{M} > 7$) are not excluded from the analysis, their occurrence is rare, and their STFs are long and complex, which means they typically do not feature a high waveform coherence with many other events. Unlike for local

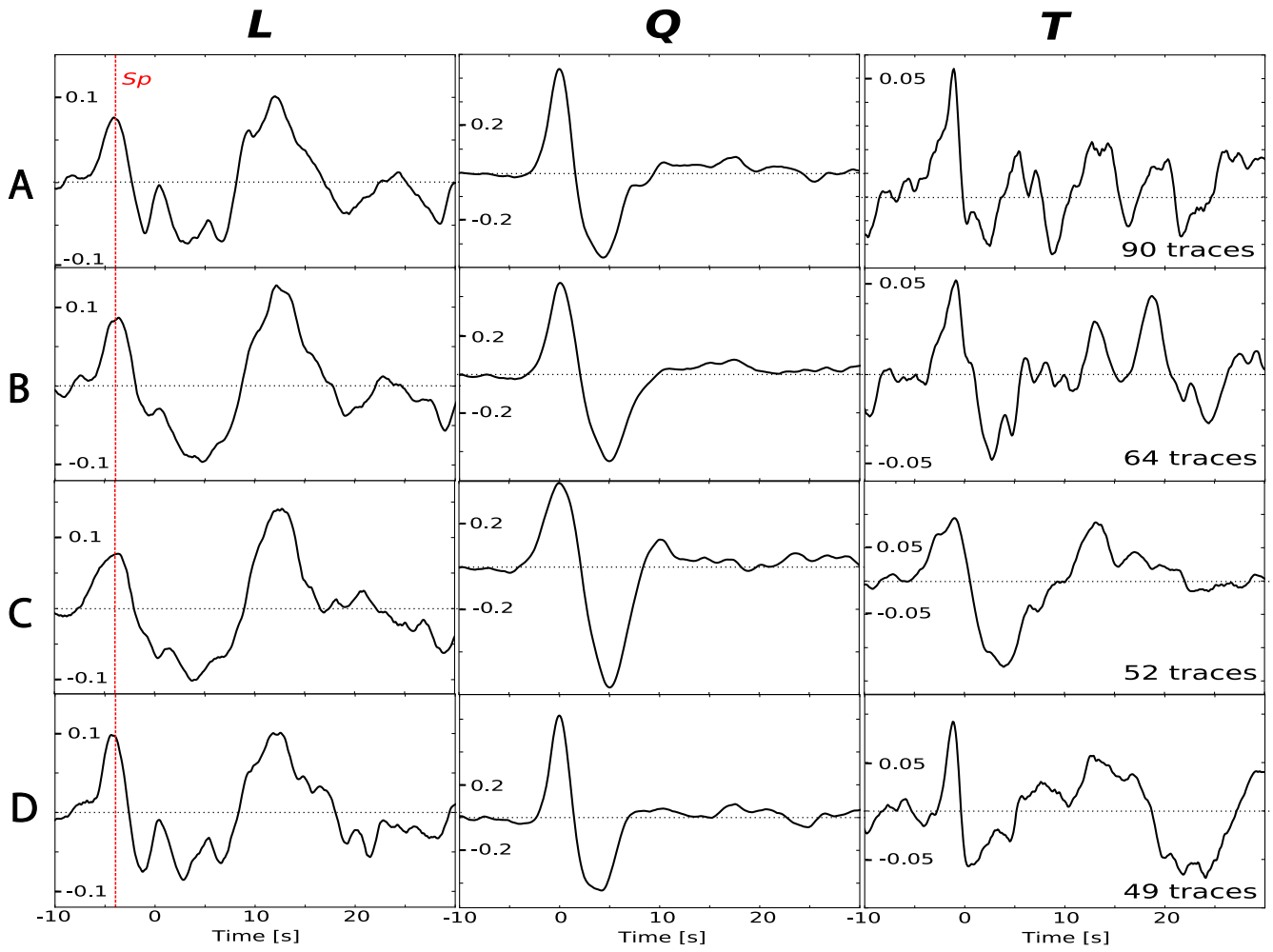


**Figure 3.** Stacked *S*-wave arrivals, obtained in the same manner as for *P*, only using a smaller window of epicentral distances (55°–75°) and rotating in the LQT coordinate system. The theoretical arrival time of the *Sp*-converted phase, computed using the model of Rai *et al.* (2003), is shown with a vertical line. The color version of this figure is available only in the electronic edition.

earthquakes, where clusters of similar waveforms usually correspond to spatially clustered events (Shearer *et al.*, 2005), signals from teleseismic earthquakes have the majority of their ray paths in the rather homogeneous mantle, thus path effects are comparatively unimportant for waveform similarity. We observe that the different stack families all show a wide geographical distribution of origin epicenters (Fig. 4a). However, it is apparent that the stacks with very sharp pulses (e.g., families C+D in Fig. 2) mainly consist of intermediate and deep-focus earthquakes (see Fig. 4b), whereas stacks with longer STFs comprise a significantly higher proportion of shallow events. Comparing our stacked waveforms to the stacks of Kumar *et al.* (2010, 2013) and Dettmer *et al.* (2015) (the last of which are overlain in Fig. 2), we see that our stacks consistently show an up-then-down STF and no evidence of a negative *P* or *S* precursor phase. These negative precursors are likely an artifact of out-of-phase stacking (see Fig. 1).

All four stacks in Figure 2 exhibit clear primary converted phases (*Ps* and *Sp*) at the expected time delays (i.e., consistent with Rai *et al.*, 2003). Reverberation phases are visible on most radial stacks, although their amplitudes are comparatively small, and they appear to arrive earlier than predicted (Fig. 2). All vertical and radial stacks show a very-long-wavelength signal after the *P* onset, which is most pronounced for stacks with long STFs corresponding to larger (shallow) earthquakes (see families A and B in Fig. 2). The period of this signal exceeds the display window in Figure 2. Because station HYB is an STS-1 seismometer with a corner period of 360 s and the filter we applied has a corner period of 100 s, we most likely see the high-frequency part of the *W* phase (Kanamori, 1993). For *S* phases (Fig. 3), sharp STFs are obtained on the Q component, with lower frequency content but of similar character (up-then-down) to the *P* pulses. The *Sp* conversion phase is observed on the L component at the expected time, whereas the consistent signal at around 0 s on the T component may indicate that the incidence angle for trace rotation was not optimal.

It should be noted that all conversion phases we retrieve mirror the shape of the original *P* pulse (or STF); that is, they are either up-then-down (*Ps*, *Ppps*) or down-then-up (*Ppss*), depending on how many reflections were encountered (see

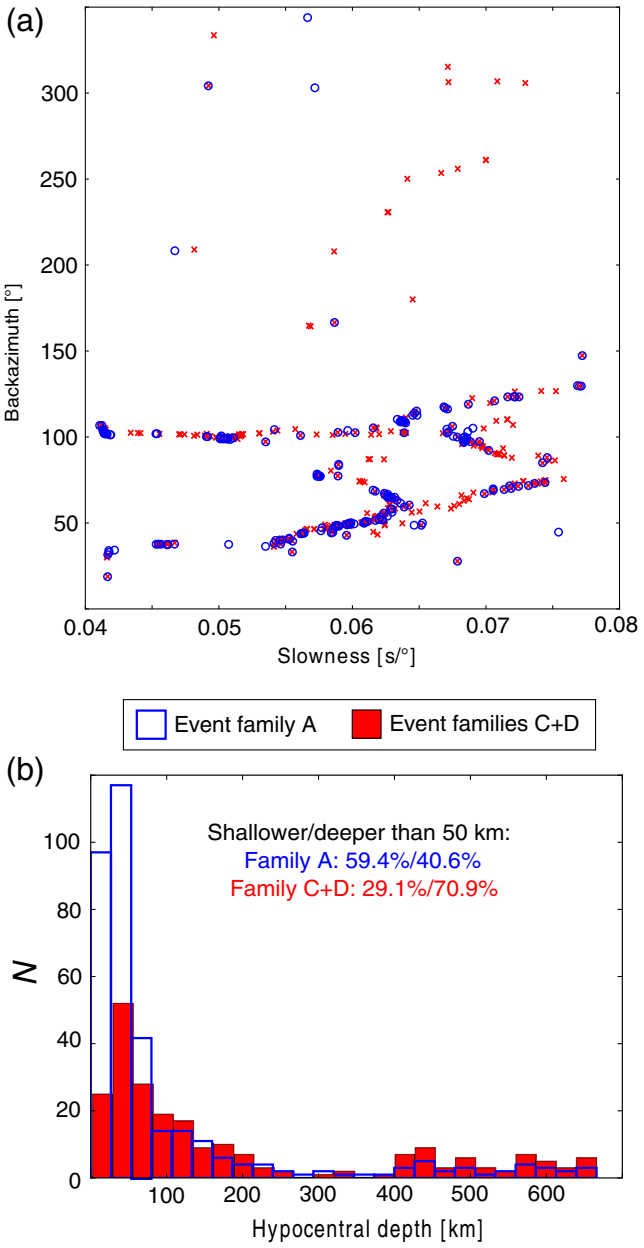


**Figure 4.** Comparison of earthquake parameters for event families A (circles and hollow bars) and C+D (crosses and filled bars) from Figure 2, which show significantly different durations of effective STFs. (a) Locations of all constituent events, shown in back-azimuth–slowness space. A clear dominance of eastern back azimuths (around 90°) is evident, which corresponds to the location of the western Pacific subduction zones. No significant spatial clustering of events or differences between the event families is discernible. (b) Hypocentral depth distribution. Event families C+D, which possess sharper and shorter effective STFs (Fig. 2), feature a significantly higher proportion of deep earthquakes. The color version of this figure is available only in the electronic edition.

insets in Fig. 2). We also retrieve a weak but discernible *PmP* phase on the vertical component, which arrives slightly earlier than predicted and is sign-reversed relative to the main *P* pulse (down-then-up). The use of this phase in structural inversion offers the potential to retrieve the $V_P$ structure of the crust, which is not possible with receiver functions. Our previous work (Dettmer *et al.*, 2015) did not show clear evidence of a *PmP* phase due to a lack of sophistication in the stacking.

## Discussion and Conclusions

The proposed method of raw seismogram stacking avoids out-of-phase stacks that create phantom phases and/or modify the pulse shape of real phases and assures that only traces with comparable STFs contribute to a stack. If a significant proportion of deep earthquakes is included in the dataset, this stacking procedure can produce sharper and shorter STFs, which is a significant advantage for inversion schemes that treat the STF as unknown and require some parametrization for it (e.g., Dettmer *et al.*, 2015). Although the approach of Kumar *et al.* (2010) produces results for the visualization of phases and their relative time differences, waveforms retrieved with that method suffer from out-of-phase stacks, which may bias inversion attempts and can result in overinterpretation of waveform complexity. Our results show that all retrieved phases possess the same wavelet shape (sign-flipped for odd numbers of reflections off a faster medium) that can be associated with the effective STF. A drawback of our method compared to stacking all available traces is that it needs a larger number of good events to identify a sufficient number of events with similar STFs for stacking. Thus, it is mainly suited for application to permanent stations with ≥5 years of high-quality data (see Ⓔ Fig. S1, available in the electronic supplement to this article, for some further examples), whereas data from temporary installations are likely unsuitable for this method and should be considered with traditional receiver function analysis.

The example in Figure 2 left back azimuth and epicentral distance (or slowness) mostly unconstrained, resulting in a large quantity of stacked traces. However, this leads to some smearing of converted phases due to different moveouts for various slownesses, as illustrated in Figure 5. In Figure 5b, one stack is subdivided into a series of stacks for different slowness bins. For instance, it is apparent that the *Ps* phase is systematically earlier for traces with lower slownesses, which widens the phase in the overall stack. Normal moveout correction is routinely used in receiver function visualization or in phase-specific stacking algorithms (e.g., Kennett, 2000). However, these moveout corrections are phase-specific; that is, because different conversion and reverberation phases have different apparent slownesses, correcting with one global moveout assumption will sharpen one phase but even further smear out another. Because structural inversion relies on the presence of a number of different phases in the seismogram, normal moveout correction is not an appropriate measure here. We thus recommend the use of narrow slowness bins to minimize the effects of normal moveout, even though this results in fewer usable data.

The fact that we retrieve not a single seismogram stack but a collection of stacks of different STFs can be exploited in structural inversion. Because each of the stacks samples the same (or at least highly similar) receiver-side structure,

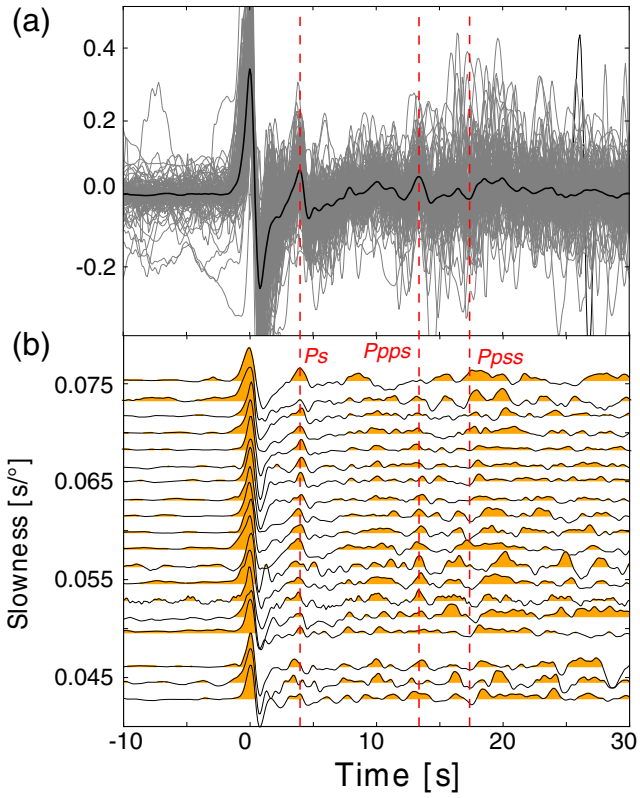


**Figure 5.** (a) Radial-component stack for *P* arrivals of event family D shown in Figure 2. All single traces contributing to the stack are shown in gray, the final stacked (and normalized) trace is shown in black. Vertical dashed lines indicate conversion and reverberation phases. (b) Traces of the stack shown in (a) are displayed in binned stacks for different slowness intervals to illustrate the effect of normal moveout. The *Ps* phase, for instance, is shown to arrive earlier for smaller slowness values. The color version of this figure is available only in the electronic edition.

but is convolved with a different STF, several stacks can be inverted separately, and the coherence between retrieved structural models can be used as validation of the inversion procedure. Alternatively, groups of stacks can be inverted jointly by treating the STF of each stack as unknown. The latter approach is desirable because it can improve resolution and reduce uncertainty in the inference of receiver-side structure. Finally, retrieval of the *PmP* phase (Fig. 2) promises better resolution of crustal *P*-wave velocity structure.

## Data and Resources

We acknowledge Incorporated Research Institutions for Seismology (IRIS) as the source of the seismogram data (http://ds.iris.edu/ds/nodes/dmc/data/, last accessed June 2016) and used event information for teleseismic earthquake from the *ISC Bulletin* (http://www.isc.ac.uk/iscbulletin/, last accessed April 2016).

## Acknowledgments

Comments by one anonymous reviewer and Associate Editor Eric Chael helped improve the article.

## References

Ammon, C. J. (1991). The isolation of receiver effects from teleseismic *P* waveforms, *Bull. Seismol. Soc. Am.* **81,** 2504–2510.

Bodin, T., M. Sambridge, H. Tkalčić, P. Arroucau, K. Gallagher, and N. Rawlinson (2012). Transdimensional inversion of receiver functions and surface wave dispersion, *J. Geophys. Res.* **117,** no. B02301, doi: 10.1029/2011JB008560.

Bodin, T., H. Yuan, and B. Romanowicz (2014). Inversion of receiver functions without deconvolution-application to the Indian craton, *Geophys. J. Int.* **196,** 1025–1033.

Dettmer, J., S. E. Dosso, T. Bodin, J. Stipčević, and P. Cummins (2015). Direct-seismogram inversion for receiver-side structure with uncertain source-time functions, *Geophys. J. Int.* **203,** 1373–1387.

Houston, H. (2001). Influence of depth, focal mechanism, and tectonic setting on the shape and duration of earthquake source time functions, *J. Geophys. Res.* **106,** 11,137–11,150.

Kanamori, H. (1993). *W* phase, *Geophys. Res. Lett.* **20,** 1691–1694.

Kennett, B. L. N. (2000). Stacking three-component seismograms, *Geophys. J. Int.* **141,** 263–269.

Kennett, B. L. N., E. Engdahl, and R. Buland (1995). Constraints on seismic velocities in the Earth from traveltimes, *Geophys. J. Int.* **122,** 108–124.

Kumar, P., R. Kind, and X. Yuan (2010). Receiver function summation without deconvolution, *Geophys. J. Int.* **180,** 1223–1230.

Kumar, P., M. Ravi Kumar, G. Srijayanthi, K. Arora, D. Srinagesh, R. K. Chadha, and M. K. Sen (2013). Imaging the lithosphere–asthenosphere boundary of the Indian plate using converted wave techniques, *J. Geophys. Res.* **118,** 5307–5319.

Langston, C. (1979). Structure under Mount Rainier, Washington, inferred from teleseismic body waves, *J. Geophys. Res.* **84,** 4749–4762.

Ligorría, J., and C. J. Ammon (1999). Iterative deconvolution and receiver-function estimation, *Bull. Seismol. Soc. Am.* **89,** 1395–1400.

Rai, S. S., K. Priestley, K. Suryaprakasam, D. Srinagesh, V. Gaur, and Z. Du (2003). Crustal shear velocity structure of the south Indian shield, *J. Geophys. Res.* **108,** 2088.

Shearer, P. (1991). Constraints on upper mantle discontinuities from observations of long-period reflected and converted phases, *J. Geophys. Res.* **96,** 18,147–18,182.

Shearer, P., E. Hauksson, and G. Lin (2005). Southern California hypocenter relocation with waveform cross-correlation, part 2: Results using source-specific station terms and cluster analysis, *Bull. Seismol. Soc. Am.* **95,** 904–915.

Vinnik, L. P. (1977). Detection of waves converted from *P* to *SV* in the mantle, *Phys. Earth Planet. In.* **15,** 39–45.

Research School of Earth Sciences
Australian National University
Building 142 Mills Road
Acton, Australian Capital Territory 2601
Australia
christian.sippl@anu.edu.au
(C.S.)

Department of Earth Science
Indian Institute of Science Education and Research
Mohanpur, Nadia 741246
Kolkata, West Bengal, India
(A.K.)

Department of Geoscience
University of Calgary
2500 University Drive Northwest
Calgary, Alberta
Canada T2N 1N4
(J.D.)

Manuscript received 25 August 2016;
Published Online 7 March 2017